Operating mechanism of the organic metal-semiconductor field-effect transistor (OMESFET)

Chang Hyun Kim, Denis Tondelier, Bernard Geffroy, Yvan Bonnassieux, Gilles Horowitz

Operating mechanism of the organic metal-semiconductor field-effect transistor (OMESFET)

Chang Hyun Kim [a,1], Denis Tondelier[1], Bernard Geffroy[1,2], Yvan Bonnassieux[1], and Gilles Horowitz[1]

[1]LPICM, Ecole Polytechnique, CNRS, 91128 Palaiseau, France

[2]CEA Saclay, DSM/IRAMIS/SPCSI/LCSI, 91191 Gif-sur-Yvette, France

(Shortened title: Operating mechanism of the OMESFET)

ABSTRACT

Organic metal-semiconductor field-effect transistors (OMESFETs) were fabricated with a polycrystalline organic semiconductor (pentacene) and characterized in order to systematically analyze their operation mechanism. Impedance measurements confirmed full depletion of the thick pentacene film (1 μm) due to the low doping concentration of unintentional doping (typically less than 10^{14} cm^{-3}). The necessity of developing a specific device model for OMESFET is emphasized as the classical (inorganic) MESFET theory based on the depletion modulation is not applicable to a fully-depleted organic semiconductor. By means of joint electrical measurements and numerical simulation, it is pointed out that the gate voltage controls the bulk-distribution of injected carriers, so that the competition between the gate and drain currents is critical for determining the operation mode. Finally, the geometrical effect is investigated with comparing a number of transistors with various channel widths and lengths.

PACS numbers: 81.05.Fb; 85.30.Tv; 72.20.-i; 85.30.Kk

[a] E-mail: chang-hyun.kim@polytechnique.edu

Phone: +33 1 69 33 43 21, Fax: +33 1 69 33 43 33

1. Introduction

Organic electronics is regarded as a future technology for the realization of low-cost, flexible devices. The recent development of organic devices such as organic light-emitting diodes (OLEDs) [1], organic thin-film transistors (OTFTs) [2], and organic photovoltaic cells (OPVs) [3] is impressive and some of them already entered into the commercial market. However, in spite of these remarkable progresses, the fundamental physics of organic devices is still incomplete, and many physical topics are highly controversial. For instance, the existence of a depletion (or space-charge) region in organic semiconductors is not a universally accepted concept until today. While the depletion region plays a key role in most classical (inorganic) semiconductor devices [4], most organic semiconductors are undoped (or unintentionally doped) and the expected depletion width normally exceeds the thickness of the semiconductor [5, 6].

This study begins from this fundamental question on the charge depletion in organic semiconductors. By characterizing pentacene-based organic diodes, it was found that pentacene diodes with the thickness up to 1 μm are fully depleted as shown by the fact that the reverse bias capacitance is voltage-independent. This result strongly motivates the development of a proper understanding of 'organic' metal-semiconductor field-effect transistor (OMESFET) because the 'inorganic' MESFET is always described with the modulation of a depletion width by the gate voltage ($\boldsymbol{V_G}$) [4].

Even though there were few recently published articles on OMESFET, physical description of the device operation was not sufficiently provided. The reported devices were fabricated with a polymeric semiconductor (poly(3-hexylthiophene)) [7, 8] or a single crystalline semiconductor (rubrene) [5]. The suggested main features of OMESFET were as follows: First, when compared to OTFTs, the OMESFET structure does not contain any insulating layer so that the intrinsic injection and transport

physics of organic semiconductors could be properly elucidated (In OTFTs, semiconductor/insulator interface dominates the device operation). Second, as the current modulation can generally be achieved within a relatively small voltage range, it could be a nice candidate for low-voltage application with fewer process steps.

Here, we report on the first experimental results of OMESFETs based on a polycrystalline organic semiconductor (pentacene). The operation mechanism of the device is systematically developed on the basis of coordinated electrical measurements and numerical simulations. It is shown that the operation of OMESFET mainly relies on the control of the distribution of injected carriers by $\boldsymbol{V_G}$. In addition, the geometrical effects is discussed by taking into account that the gate current ($\boldsymbol{I_G}$) and the drain current ($\boldsymbol{I_D}$) are in competition for charge transports.

2. Experimental

Organic diodes and OMESFETs were fabricated according to the same process run, following the structures depicted in Figure 1. Subsequently evaporated Au (anode), pentacene (organic semiconductor), and Al (cathode) make up a metal-semiconductor-metal (MSM) type organic diode. An OMESFET consists of two organic diodes with a common semiconductor layer and a common top ‘gate’ electrode. The two separated bottom electrodes are denoted as ‘source’ and ‘drain’.

All evaporation processes were done under a pressure of about 2×10^{-7} mbar with the substrate kept at room temperature. The evaporation rate of pentacene was 0.1 nm/sec with a final thickness of 1 μm for both the organic diodes and OMESFETs.

Current-voltage (I-V) measurements were carried out using a semiconductor characterization system (Keithley 4200) and impedance measurements were conducted using a HP 4192A LF impedance analyzer. All electrical measurements were done in the dark at room temperature. Tapping-mode

atomic force microscopy (AFM) images of pentacene were taken using Veeco Dimension 5000 AFM system.

3. Results and discussion

3.1. Full depletion in unintentionally doped pentacene

Organic diodes can serve as a starting point for understanding the OMESFET because as explained in Section 2, the OMESFET is the superposed structure of two organic diodes. A representative current-voltage characteristic (I-V) of the pentacene diode (active area: 4.3×10^{-4} cm^2) is shown in Figure 2. The inset shows the polycrystalline morphology of the deposited pentacene (1 μm-thick) layer on Au electrode (AFM scan size: 2×2 μm^2).

In order to accurately understand the I-V curves, it is worth reminding the relative position of energy levels of each material. Au electrode favors hole injection into the HOMO of pentacene because the work function of (not atomically clean) Au is 4.9 eV while the ionization potential of pentacene is 5.2 eV (the resulting injection barrier is 0.3 eV). By contrast, Al is a low-work function metal (4.2 eV) and it cannot supply significant amount of either type of carriers into the HOMO or LUMO of pentacene (the electron affinity of pentacene is 2.8 eV). As a result, the I-V curve is inevitably asymmetric and a strong rectification behavior is obtained.

The applied voltage ($\boldsymbol{V_a}$) in Fig. 2 corresponds to the voltage at the Au electrode (anode) with the Al electrode (cathode) grounded. As expected from the energy levels, the current in the reverse-bias regime ($\boldsymbol{V_a} < 0$ V) is extremely low due to the low current injection at the Al contact. Under forward-bias ($\boldsymbol{V_a} > 0$ V), the current starts to increase exponentially (injection-limited current) owing to the

injected holes from Au electrode and when the voltage becomes higher than the built-in potential, the current is determined by the bulk conductivity of the semiconductor (bulk-limited current) [9, 10].

Since the diode characteristics resemble that of (inorganic) Schottky diodes and the physics of organic diodes is not yet fairly established, the current trend is to adopt the Schottky model to interpret the experimental data of organic diodes [11-14]. However, we could confirm by means of impedance-voltage (Z-V) measurements that the pentacene layer is fully depleted so that the Schottky model is not appropriate in that case.

Figure 3 is the impedance-voltage (Z-V) curve of the same pentacene diode. Two distinguishable regimes (reverse and forward regimes) are also observed in this graph. Under reverse-bias, the device is a perfect capacitor as the measured phase angle is constant as -90 degrees [15]. Furthermore, the capacitance does not depend of the applied reverse-bias (the impedance modulus is constant). This is at variance with the case of the Schottky diode, where the reverse-bias 'depletion' capacitance depends on the applied voltage as the depletion width is modulated by the applied voltage [4]. In the forward-bias regime, the device becomes more resistive (the phase angle approaching 0 degree) as a consequence of the rising current flow.

The observed voltage-independent reverse-capacitance is a clear evidence for the 'full' depletion of the thick pentacene layer. Keeping in mind that the depletion width is determined by the doping concentration, it points out that the doping concentration of pentacene layer is so low that the expected depletion width (by calculation) exceeds the whole thickness of the semiconductor.

Pentacene, along with many other reported organic semiconductors, is described as an 'unintentionally' doped semiconductor because some chemical reactions with ambient air or the presence of residues of its chemical synthesis could introduce dopant-like species, most often in an uncontrollable manner [16]. In order to further associate the observed full depletion of pentacene with the unintentional doping, physically-based two-dimensional device simulation (ATLAS simulator by

SILVACO, Inc.) was conducted. This simulation involves solving under a finite-element framework a set of coupled Poisson's, continuity and transport equations (drift-diffusion model in this case) within the defined two-dimensional device structure.

Figure 4 is the simulated potential profiles in the pentacene organic diode at thermal equilibrium ($\boldsymbol{V_a}$=0 V) by ATLAS simulation. The above-mentioned energy levels of Au, pentacene, and Al are taken for the calculation and the reference potential (0 V) is that of the cathode. It should be noted that as long as the doping concentration lies under 10^{14} cm^{-3} the potential profiles are straight lines and do not show the quadratic shape that characterize the presence of a depletion region (full depletion). This indicates that a fully depleted MSM diode has in fact the energy diagram of a metal-insulator-metal (MIM) capacitance without any band bending. The potential difference between the two electrodes corresponds to the built-in (or diffusion) potential, which stems from the work function difference of the two metals (0.7 eV). When the doping concentration increases up to 10^{16} cm^{-3}, the diode becomes a Schottky-type diode with a visible depletion region located at the pentacene/Al contact (larger Fermi-level mismatch exists here). The simulation confirms that for doping concentrations lower than 10^{14} cm^{-3}, full depletion of the 1 μm-thick pentacene film takes place. Importantly, this also implies that the current flow in organic diodes is entirely due to charge carriers 'injected' from the electrode because there are practically no 'thermally generated' carriers in the pentacene layer.

3.2. Operation mechanism of the OMESFET

The experimentally-proved full depletion of pentacene infers a specific device model for the OMESFET because inorganic MESFET operates through the depletion modulation by $\boldsymbol{V_G}$ [4]. This Section presents the experimental data of pentacene OMESFETs together with physical simulations that will explain its operation under different biasing conditions.

Figure 5 shows the diodes characteristics of a representative pentacene OMESFET with a channel width (W) of 400 μm and a channel length (L) of 50 μm (the inset is the microscope image of the device). As indicated in the cross-sectional view of the OMESFET in Fig. 1, two organic diodes are formed between the gate electrode and the two bottom electrodes, respectively. From the I-V curves in Fig. 5, one can obviously see that these two diodes are equivalent. V_G and the drain voltage (V_D) are the relative potentials to the grounded source electrode. Note that V_G is now applied to the Al electrode, so that the diodes in the OMESFET are 'forward'-biased when V_G is negative as shown in Fig. 5.

In Figure 6, output characteristics (I_D-V_D) are presented with different V_G values. The transistor functions as a normally-on device (non-zero current at V_G=0 V) and the current modulation is observed over a very small range of V_G. In order to investigate the role of V_G in OMESFETs, the structure was simulated with ATLAS as it allows to explore various physical information inside the semiconductor. Figure 7 contains a two-dimensional contour mapping of the hole concentration (in log scale) in the pentacene layer with different bias conditions. It should be kept in mind that the hole concentration at the metal-semiconductor interface is determined by the injection barrier; the concentration is high at the source/drain electrode (Au) but negligibly low at the gate electrode (Al) and these 'interface' features do not depend on the bias conditions (Fig. 7. (a), (b), and (c)). However, V_G controls the distribution of injected holes inside the semiconductor layer, so that one can see significant changes of the hole concentration in the volume of the semiconductor. When a positive V_G is applied (Fig. 7. (a)), the 'bulk' conductivity of pentacene is lowered (lower hole concentration) and the current is lowered as well (Fig. 6). A negative V_G functions inversely (Fig. 7. (c)); it draws the injected holes toward the gate electrode the conductivity and the current increase as a result (Fig. 6).

Figure 8 shows the measured transfer characteristics (I_D-V_G) of the same transistor. As V_G decreases toward the negative regime, I_D increases steadily but below a given value, I_D starts to sharply decrease. The normal-operation regime (V_G lower than about -1 V) is already explained in Figs. 6 and 7

by the V_G-controlled bulk conductivity. To help understand the reason for the abrupt decline of I_D, another set of simulation is provided in Figure 9. This figure shows the hole current density ($Jh+$) contour map as well as vectors indicating the direction and magnitude of $Jh+$. One should focus the attention on the current vectors in the region between the gate and the drain electrodes (the right side of the structure). When V_G=-1 V (Fig. 9. (a)), current vectors in this region are directed toward the drain electrode. With V_G=-2 V (Fig. 9. (b)), vectors of opposite directions are compensating each other so that the net current in this region is negligible. Finally, when V_G =-3 V (Fig. 9. (c)), all the vectors are pointing toward the gate electrode because now the gate-drain diode is forward-biased. The above discussion can be otherwise explained by the competition between I_D and I_G. Because of the absence of a gate insulator which can block the current toward the gate, I_G and I_D are in competition. It means that when V_G is too high (negatively), all carriers tend to transport toward the gate (I_G becomes dominant) and I_D decreases dramatically. The polarity of I_D can be even reversed with higher V_G (the negative I_D in Fig. 8 corresponds to the net current flowing 'into the drain' and the positive I_D mirrors the net current coming 'out of the drain').

Due to the above-detailed mechanisms with competing I_D and I_G, the allowed operation regime of OMESFET should be limited within low V_G range for 'normal' operation.

3.3. Effect of the device geometry

The model of the metal-insulator-semiconductor field-effect transistor (MISFET) (including the TFT structure) leads to I-V equations with a geometrical scaling factor equal to the ratio of W to L where the drain current is expected to be proportional to this W/L ratio. In this Section, the influence of the channel geometry in OMESFET is discussed by separately varying W and L and monitoring the

change of I_D. The results revealed that I_D in an OMEFSET does not follow the simple linear relationship with W and L.

In Figure 10 (a), the output curves of four different transistors with L=40, 60 , 80, and 100 μm are depicted with the same W (400 μm). I_D tends to decrease as the channel becomes longer, like in MISFETs. A simple explanation is that because L represents the spacing between source and drain, the longitudinal electric field strength is a decreasing function of L for the same V_D. The variation of I_D is then plotted taking L as a variable (Fig. 10. (b)). I_D is monotonously decreasing with increasing L but the graph is not perfectly linear. This non-linearity is accounted for by the fact that the MESFET is a bulk-type device while the MISFET involves surface conduction at the semiconductor/insulator interface. The current in OMESFET is not confined at the interface; rather, it is distributed in the whole semiconductor bulk as shown in Fig. 9. As a consequence, the integrated trajectories of all current components cannot be perfectly proportional to the channel spacing and the I_G component that always exists makes the dependence more complicated (The insulator blocks I_G in case of MISFET).

As the effect of the channel 'length' is well explained, another set of results on the effect of channel 'width' is now presented (Figure 11). This W-dependence on I_D gives important insight for OMESFET operation. The three output curves in Fig. 11. (a) are those of transistors with W=400, 1000, and 1500 μm with L=30 μm. The current is lower with larger channels and this is the opposite of what is expected for MISFETs. Fig. 11 (b) shows well that I_D abruptly decreases with increasing W and even goes to nearly zero with 1500-μm channel. This effect could be explained by the current competition between I_D and I_G (described in Section 3.2). The reason why I_D in MISFETs is proportional to W is that the current cross section (the area through which the current passes) is larger with bigger W and it seems to be also true in MESFET. However, in our MESFET structure, there is another factor that intervenes in the situation; the current cross section from the source/drain to the gate also linearly increases with W. Even though both cross sections for I_D and I_G are simultaneously increasing with W

the contribution for I_G is much stronger because the source-gate electric field is much stronger than the source-drain electric field with similar order of V_G and V_D (the thickness of pentacene is 1 μm and the source-drain spacing (L) is 30 μm). In other words, increasing W cannot possibly favor any increase of I_D because the 'greatly' increasing I_G component 'strongly' depresses the current flow toward the drain and even leads to the decrease of I_D.

4. Conclusion

The operation mechanism of OMESFET was elucidated by simultaneously characterizing and simulating pentacene-based OMESFETs. The full depletion of 1 μm-thick pentacene diode was proved by impedance analysis and this result confirmed very low unintentional doping concentrations (less than 10^{14} cm^{-3}). In an attempt to model the OMESFET excluding depletion modulation, measured output and transfer characteristics were analyzed with the physical pictures obtained by the two-dimensional device simulations. The proper function of V_G was identified as a control of the distribution of injected carriers which determines the bulk conductivity. The limitation of operation mode was then emphasized by taking into account the competition between I_G and I_D in the absence of an insulating layer. In order to further investigate the behavior of OMESFET, channel geometry-dependent I-V characteristics were dealt with by systematically comparing a number of devices with different W and L. The results showed that small transistor is desirable for expecting high I_D because the I_D decreases as both W and L increase. From this comprehensive study on OMESFET, the overall operation of OMESFET is well understood and we expect that this will help for the further modelling and application of the OMESFETs.

ACKNOWLEDGEMENTS

This study was supported by the NoE POLYNET from the European Community's Seventh Framework Program (FP7/2007-2013) under grant agreement n° 214006. C. H. Kim thanks the Vice Presidency for External Relations (DRE) in Ecole Polytechnique for the Ph.D. fellowship.

REFERENCES

1. S. Chen, L. Deng, J. Xie, L. Peng, L. Xie, Q. Fan, W. Huang, Adv. Mater. **22**, 5227 (2010)

2. D. Braga, G. Horowitz, Adv. Mater. **21**, 1473 (2009)

3. G. Dennler, M. C. Scharber, C. J. Brabec, Adv. Mater. **21**, 1323 (2009)

4. S. M. Sze, K. K. Ng, *Physics of Semiconductor Devices*, 3rd edn. (Wiley-Interscience, New York, 2007)

5. D. Braga, M. Campione, A. Borghesi, G. Horowitz, Adv. Mater. **22**, 424 (2010)

6. W. Brütting, S. Berleb, A. G. Mückl, Org. Electron. **2**, 1 (2001)

7. A. Takshi, A. Dimopoulos, J. D. Madden, Appl. Phys. Lett. **91**, 083513 (2007)

8. A. Takshi, A. Dimopoulos, J. D. Madden, IEEE Trans. Electron Devices **5**, 276 (2008)

9. K. C. Kao, W. Hwang, *Electrical Transport in Solids with Particular Reference to Organic Semiconductors* (Pergamon Press, London, 1981)

10. P. Mark, W. Helfrich, J. Appl. Phys. **33**, 205 (1962)

11. P. Stallinga, H. L. Gomes, M. Murgia, K. Müllen, Org. Electron. **3**, 43 (2002)

12. E. J. Lous, P. W. M. Blom, L. W. Molenkamp, D. M. de Leeuw, Phys. Rev. B **51**, 17251 (1995)

13. T. Kaji, T. Takenobu, A. F. Morpurgo, Y. Iwasa, Adv. Mater. **21**, 3689 (2009)

14. Y. S. Lee, J. H. Park, J. S. Choi, Opt. Mater. **21**, 433 (2002)

15. C. K. Alexander, M. N. O. Sadiku, *Fundamentals of Electric Circuits*, 2nd edn. (McGraw-Hill, New York, 2004)

16. O. D. Jurchescu, J. Baas, T. T. M. Palstra, Appl. Phys. Lett. **87**, 052102 (2005)

FIGURE CAPTIONS

Figure 1. Devices structure of the organic diode and the OMESFET adopted in this study.

Figure 2. Representative I-V characteristic of pentacene-based organic diode on semi-logarithmic plot. Inset shows the AFM morphology of 1 μm-thick pentacene film on Au bottom electrode.

Figure 3. Impedance-voltage (Z-V) data showing fully depleted organic layer at the reverse-bias regime.

Figure 4. Simulated potential profiles by ATLAS showing variation of the potential profiles as setting different (p-type) doping concentration into the simulator ($\boldsymbol{V_a}$=0 V).

Figure 5. Diode characteristics in an OMESFET device measured from a gate-source biasing (G-S diode) and a gate-drain biasing (G-D diode). Inset is the optical microscopic image of this OMESFET ($\boldsymbol{W}$=400 μm and $\boldsymbol{L}$=50 μm).

Figure 6. Output characteristics ($\boldsymbol{I_D}$-$\boldsymbol{V_D}$) of the OMESFET.

Figure 7. Simulated two-dimensional structures of the OMESFET showing the variation of hole concentration in the pentacene layer with (a) $\boldsymbol{V_G}$=0.8 V, (b) $\boldsymbol{V_G}$=0 V, and (c) $\boldsymbol{V_G}$=-0.8 V.

Figure 8. Transfer characteristics ($\boldsymbol{I_D}$-$\boldsymbol{V_G}$) of the OMESFET. Two operation regimes are indicated; the normal-operation regime with proper I_D modulation by $\boldsymbol{V_G}$, the $\boldsymbol{I_G}$-dominant regime where $\boldsymbol{I_D}$ is depressed by strong $\boldsymbol{I_G}$ component.

Figure 9. Simulated two-dimensional structures of the OMESFET showing the hole current density (contours and vectors) in the pentacene layer with different biasing conditions; (a) $\boldsymbol{V_G}$=-1 V, $\boldsymbol{V_D}$=-2 V, (b) $\boldsymbol{V_G}$=-2 V, $\boldsymbol{V_D}$=-2 V, and (c) $\boldsymbol{V_G}$=-3 V, $\boldsymbol{V_D}$=-2 V.

Figure 10. Geometrical effect of the channel length on the current; (a) output characteristics of four OMESFETs with $\boldsymbol{W}$=400 μm and $\boldsymbol{L}$=40, 60, 80, 100 μm, (b) $\boldsymbol{I_D}$-$\boldsymbol{L}$ plots.

Figure 11. Geometrical effect of the channel width on the current; (a) output characteristics of three OMESFETs with $\boldsymbol{L}$=30 μm and $\boldsymbol{W}$=400, 1000, 1500 μm, (b) $\boldsymbol{I_D}$-$\boldsymbol{W}$ plots.

Figure 1

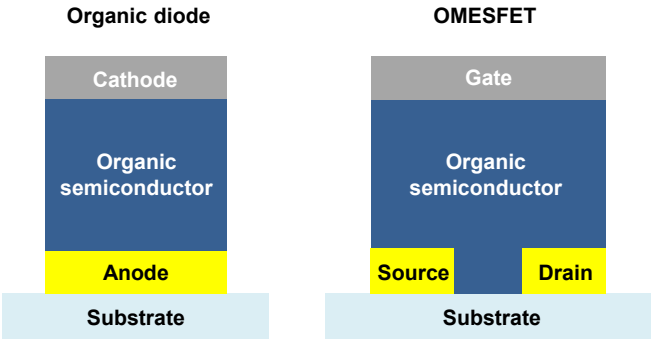
Organic diode
Cathode
Organic semiconductor
Anode
Substrate
OMESFET
Gate
Organic semiconductor
Source
Drain
Substrate

Figure 2

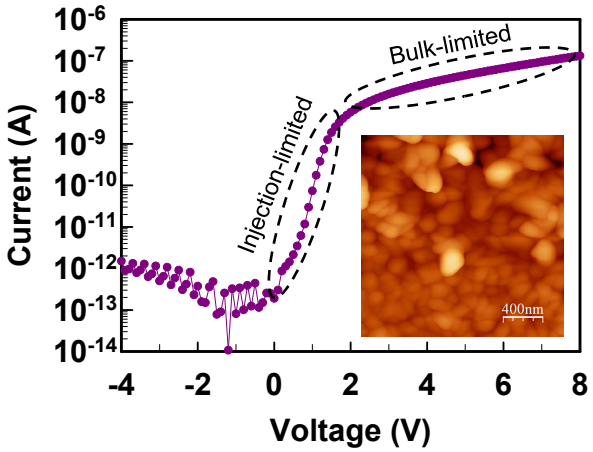
Current (A)
10-6
10-7
10-8
10-9
10-10
10-11
10-12
10-13
10-14
-4
-2
0
2
4
6
8
Voltage (V)
Bulk-limited
Injection-limited
400nm

Figure 3

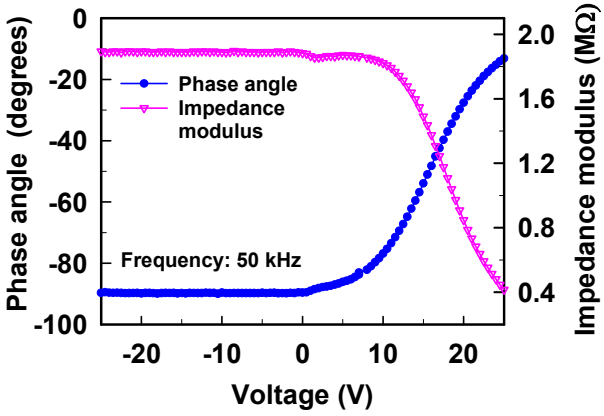
Phase angle (degrees)
0
-20
-40
-60
-80
-100
Impedance modulus (MΩ)
2.0
1.6
1.2
0.8
0.4
Phase angle
Impedance modulus
Frequency: 50 kHz
-20
-10
0
10
20
Voltage (V)

Figure 4

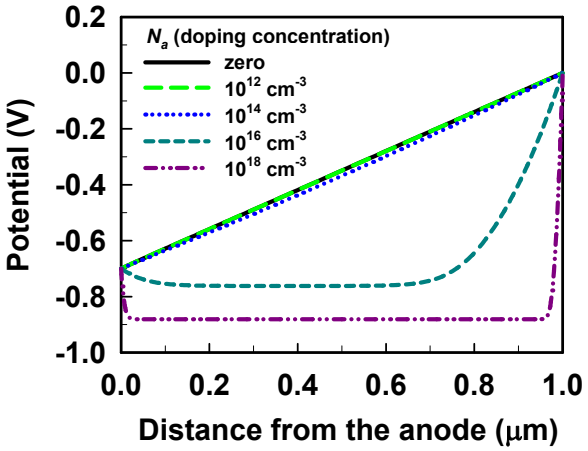
N_a (doping concentration)
zero
10^{12} cm^{-3}
10^{14} cm^{-3}
10^{16} cm^{-3}
10^{18} cm^{-3}
Potential (V)
0.2
0.0
-0.2
-0.4
-0.6
-0.8
-1.0
0.0
0.2
0.4
0.6
0.8
1.0
Distance from the anode (μm)

Figure 5

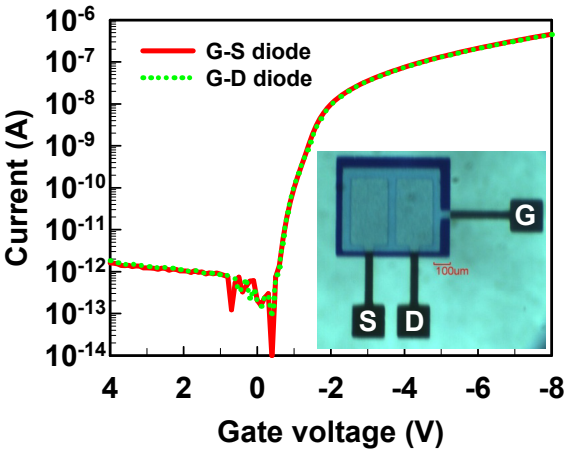
G-S diode
G-D diode
Current (A)
10-6
10-7
10-8
10-9
10-10
10-11
10-12
10-13
10-14
4
2
0
-2
-4
-6
-8
Gate voltage (V)
G
S
D
100um

Figure 6

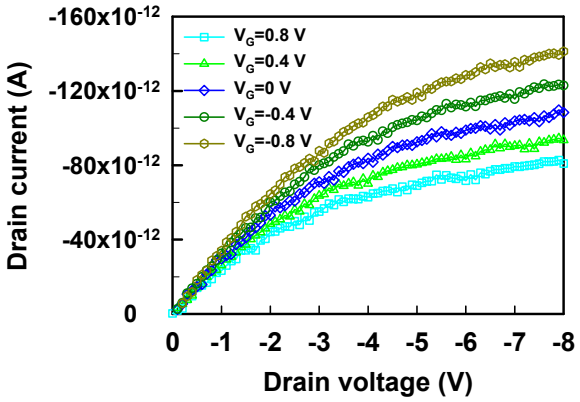
-160x10-12
-120x10-12
-80x10-12
-40x10-12
0
Drain current (A)
VG=0.8 V
VG=0.4 V
VG=0 V
VG=-0.4 V
VG=-0.8 V
0
-1
-2
-3
-4
-5
-6
-7
-8
Drain voltage (V)

Figure 7

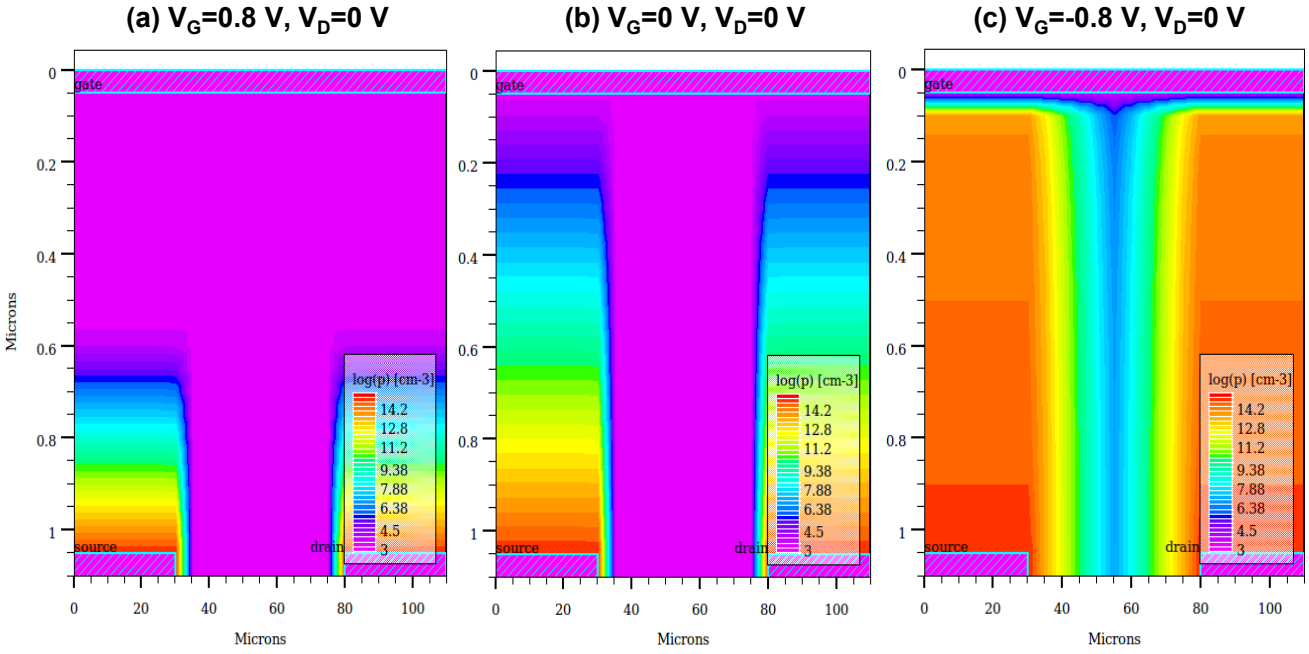
(a) V_G=0.8 V, V_D=0 V
(b) V_G=0 V, V_D=0 V
(c) V_G=-0.8 V, V_D=0 V
gate
source
drain
log(p) [cm-3]
14.2
12.8
11.2
9.38
7.88
6.38
4.5
3
Microns
0
0.2
0.4
0.6
0.8
1
0
20
40
60
80
100

Figure 8

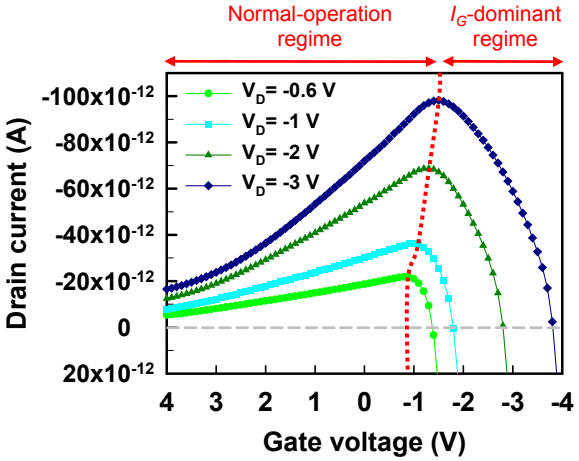
Normal-operation regime
I_G-dominant regime
V_D= -0.6 V
V_D= -1 V
V_D= -2 V
V_D= -3 V
Drain current (A)
-100x10^{-12}
-80x10^{-12}
-60x10^{-12}
-40x10^{-12}
-20x10^{-12}
0
20x10^{-12}
4 3 2 1 0 -1 -2 -3 -4
Gate voltage (V)

Figure 9

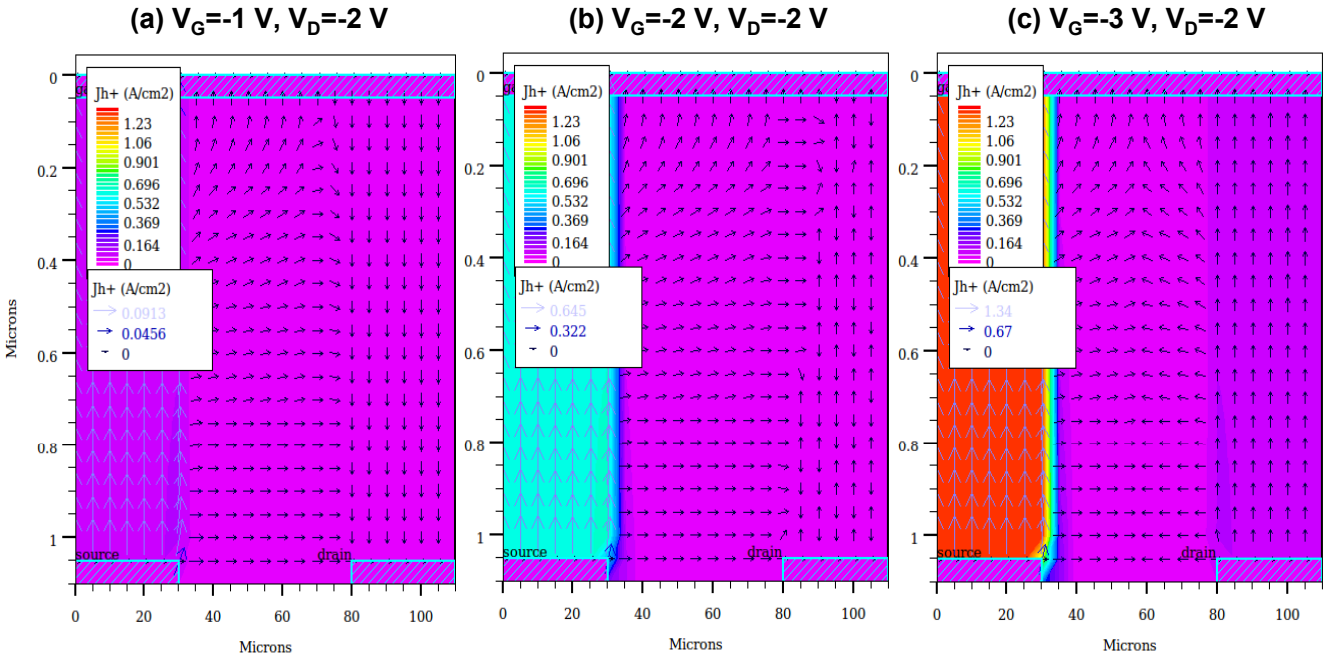
(a) V_G=-1 V, V_D=-2 V
(b) V_G=-2 V, V_D=-2 V
(c) V_G=-3 V, V_D=-2 V
Jh+ (A/cm2)
1.23
1.06
0.901
0.696
0.532
0.369
0.164
0
Jh+ (A/cm2)
0.0913
0.0456
0
Jh+ (A/cm2)
0.645
0.322
0
Jh+ (A/cm2)
1.34
0.67
0
source
drain
Microns
Microns

Figure 10

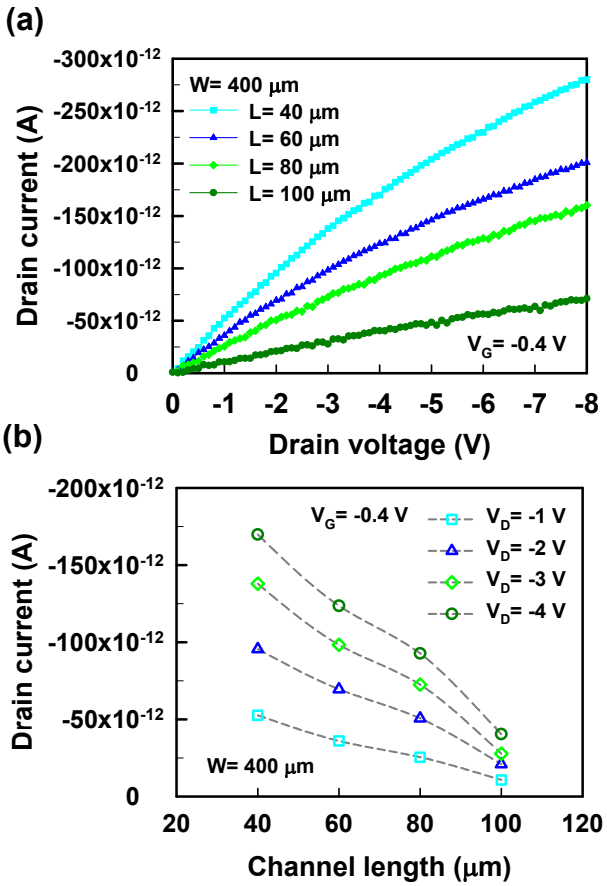
(a)
-300x10-12
-250x10-12
-200x10-12
-150x10-12
-100x10-12
-50x10-12
0
Drain current (A)
W= 400 μm
L= 40 μm
L= 60 μm
L= 80 μm
L= 100 μm
VG= -0.4 V
0 -1 -2 -3 -4 -5 -6 -7 -8
Drain voltage (V)
(b)
-200x10-12
-150x10-12
-100x10-12
-50x10-12
0
Drain current (A)
VG= -0.4 V
VD= -1 V
VD= -2 V
VD= -3 V
VD= -4 V
W= 400 μm
20 40 60 80 100 120
Channel length (μm)

Figure 11

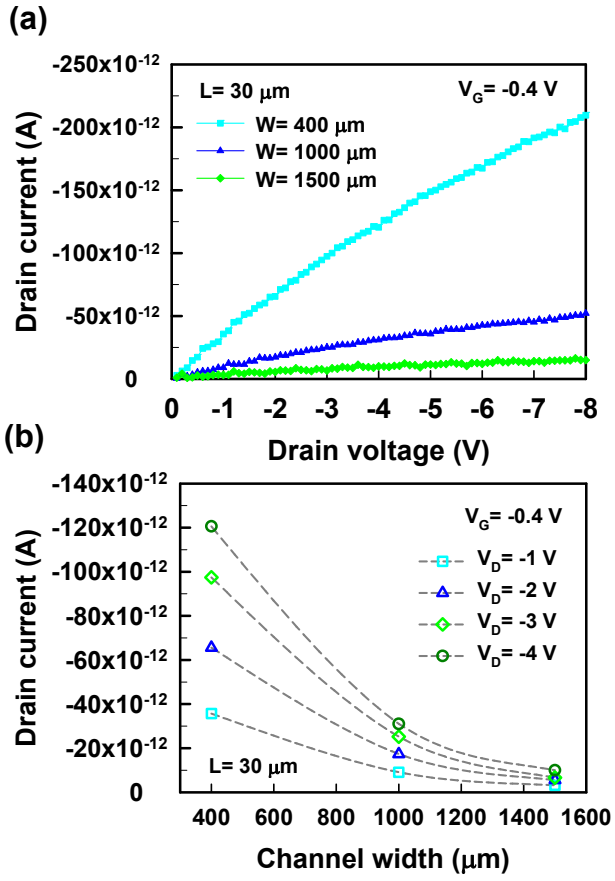
(a)
L= 30 μm
V_G= -0.4 V
W= 400 μm
W= 1000 μm
W= 1500 μm
Drain current (A)
-250x10-12
-200x10-12
-150x10-12
-100x10-12
-50x10-12
0
0 -1 -2 -3 -4 -5 -6 -7 -8
Drain voltage (V)
(b)
V_G= -0.4 V
V_D= -1 V
V_D= -2 V
V_D= -3 V
V_D= -4 V
L= 30 μm
Drain current (A)
-140x10-12
-120x10-12
-100x10-12
-80x10-12
-60x10-12
-40x10-12
-20x10-12
0
400 600 800 1000 1200 1400 1600
Channel width (μm)